



Fallon, E. K., Niehorster, E., Brooker, R. A., & Scott, T. B. (2018). Experimental leaching of massive sulphide from TAG active hydrothermal mound and implications for seafloor mining. *Marine Pollution Bulletin*, 126, 501-515.
<https://doi.org/10.1016/j.marpolbul.2017.10.079>

Peer reviewed version

License (if available):
CC BY-NC-ND

Link to published version (if available):
[10.1016/j.marpolbul.2017.10.079](https://doi.org/10.1016/j.marpolbul.2017.10.079)

[Link to publication record in Explore Bristol Research](#)
PDF-document

This is the author accepted manuscript (AAM). The final published version (version of record) is available online via ELSEVIER at <https://www.sciencedirect.com/science/article/pii/S0025326X17309256?via%3Dihub>. Please refer to any applicable terms of use of the publisher.

University of Bristol - Explore Bristol Research

General rights

This document is made available in accordance with publisher policies. Please cite only the published version using the reference above. Full terms of use are available:
<http://www.bristol.ac.uk/red/research-policy/pure/user-guides/ebr-terms/>

1 Experimental leaching of sulphide ore from TAG hydrothermal mound and implications 2 for seafloor massive sulphide mining

3
4 **Emily K Fallon**^{1,2}, Ella Niehorster¹, Richard A Brooker², Thomas B Scott¹,

5 ¹ Interface Analysis Centre, School of Physics, HH Wills Physics Laboratory, Tyndall Ave. University of Bristol, BS8
6 1TL. UK.

7 ² School of Earth Sciences, Wills Memorial Building, Queens Rd, University of Bristol, BS8 1RJ. UK.

8
9 *Current address to which correspondence should be sent; Interface Analysis Centre, School of Physics, HH Wills
10 Physics Laboratory, Tyndall Ave. University of Bristol, BS8 1TL. UK.

11 Tel. (44) 117 3317685

12 Email. e.fallon@bristol.ac.uk

13 14 **Abstract**

15 Seafloor massive sulphide (SMS) samples from the Trans-Atlantic Geotraverse deposit on the Mid-Atlantic Ridge
16 were characterised and subjected to leaching experiments to emulate proposed SMS mining processes. Over
17 time, leached Fe is removed from solution by the precipitation of Fe oxy-hydroxides, whereas Cu and Pb leached
18 remained in solution at ppb levels. Bulk chemistry is not the main control on leachate concentrations; instead
19 mineralogy and/or galvanic couples between minerals are the driving forces behind the type and concentration of
20 leached metals. Dissolved concentrations exceed ANZECC toxicity guidelines by 620 times, implying the formation
21 of localised toxicity in a stagnant water column. Moreover, concentrations will be higher when scaled to higher
22 rock-fluid ratios and finer grain sizes proposed for mining scenarios. The distance at which dilution is achieved to
23 meet guidelines is unlikely to be sufficient, indicating a need for the refinement of the mining process.

24 25 **Keywords**

26 SMS deposits

27 Mining impact

28 Leaching

29 Metal release

30 Toxicity

31 **1 Introduction**

32 As the global demand for metals continues to grow, driven by advances in technology, so does the market price.

33 With the majority of economically viable terrestrial resources already exploited and fewer being discovered,

34 previously disregarded sources of metals are now beginning to be more seriously considered. Heightened interest

35 in seafloor exploration is highlighted by governments and commercial enterprises already applying for and

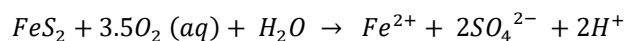
36 receiving licenses for exploration, with 26 exploration licences issued by the International Seabed Authority (ISA)

37 as of July 2015, covering 1.2 million square kilometres of the seafloor ((ISA), 2016). Additionally, there are an
38 estimated 26 exploration projects within national jurisdiction areas of individual states' economic exclusion zones
39 (EEZs) (ECORYS, 2014). Further to this, 77 submissions have been made by 67 different territories to extend their
40 continental shelf and subsequently their economic exclusion zone to lay claim to larger expanses of the seafloor
41 and associated mineral resources ((CLCS), 2016). Advances in deep-sea oil and gas extraction technology have
42 paved the way for the economic viability of deep-sea mining. As a result, expectations are high that this industry is
43 about to emerge.

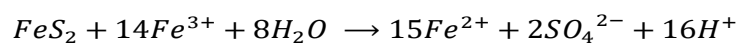
44
45 Seafloor massive sulphide (SMS) ore deposits and their economic worth has been discussed extensively in the
46 literature (German et al., 2016; Hannington and Jamieson, 2011; Hannington et al., 2010; Monecke et al., 2016),
47 with Nautilus Minerals Inc. already in the process of commencing mineral extraction in what would be the world's
48 first SMS mine at the Solwara 1 deposit in the Bismarck Sea off Papua New Guinea. In order to support any future
49 economic potential, our knowledge and understanding of such deposits requires significant improvement with an
50 associated need for assessment of any environmental impact that any future endeavours may produce.

51
52 Sulphide minerals at both active and inactive hydrothermal seafloor vents undergo chemical interaction with
53 seawater. This generally results in oxidative weathering (Edwards, 2004a), a process similar to the weathering that
54 occurs in their terrestrial counterparts – volcanogenic massive sulphide (VMS) deposits. On land in restricted
55 drainage systems, this occurs more vigorously at decreasing values of pH and can result in acid mine drainage
56 (AMD), which promotes further dissolution as shown for pyrite in Eq. 1 & 2.

57
58 **Equation 1**



59
60
61
62 **Equation 2**

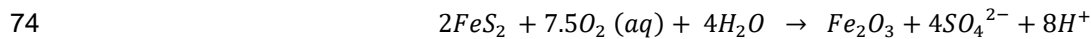


63
64

65 In contrast, this equivalent weathering process on the seafloor occurs in waters of near neutral pH and of almost
66 'infinite' volume, so that arising acidity from oxidation is almost immediately buffered and low pH conditions will not
67 develop over a significant area due to the dilution effect. The reactions result in formation of insoluble oxy-
68 hydroxide minerals such as goethite and hematite at the expense of sulphides such as pyrite; as illustrated in Eq.
69 3 & 4 (Mills and Elderfield, 1995; Edwards, 2004). These Fe oxide minerals can accumulate as crusts or caps on
70 sulphide deposits on the seafloor and are referred to as 'gossans' with the mineral mixtures often referred to as
71 limonite (Herzig and Hannington, 1995).

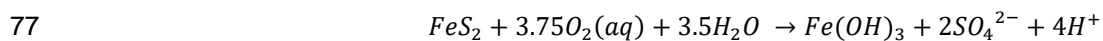
72

73 Equation 3



75

76 Equation 4



78

79

80

81 Based on the natural seafloor weathering process, it is argued that any exposure of sulphide as a result of mining
82 will have a similar effect: with negligible net release of metals and pH that is buffered to neutral. However, the
83 process of deep-sea mining has the potential to expose a high surface area of fresh sulphide minerals to the
84 corrosive effects of seawater, allowing for an anthropogenic leaching of metals that is more akin to acid mine
85 drainage observed in a terrestrial setting (Gwyther, 2008; Parry, 2008; Simpson et al., 2007). The only current
86 concept for SMS mining is provided by Nautilus Minerals Inc. and includes an 'in situ' extraction phase that
87 produces 80% <25mm and 20% smaller unknown particle size material, (where 30% of cut material is initially lost
88 and up to 10% will remain on the seafloor). This is combined with a dewatering process that occurs as the mineral
89 slurry (1:9 rock to fluid ratio) is carried to the surface, processed above sea level, and the waste water is returned
90 to 25 to 50 m above the seafloor containing <8 µm sulphide particles at 6.35 g/L rock to fluid ratio. Both 'in situ'
91 extraction and dewatering involve the entrainment of fresh sulphide material into an advective environment, with
92 the dewatering process also providing exposure of sulphide to warmer temperature at the sea surface.

93

94 If any leaching of metals is not balanced by precipitation of oxides, there is the potential for local accumulation of
95 dissolved heavy metals in the water column. These metals may bio accumulate in local ecosystems, disperse or
96 accumulate in the wider ocean or ultimately precipitate elsewhere as oxides. As SMS deposits have been around
97 for most of the Earth's history, it might be assumed there is equilibrium established between weathering processes
98 and the local bio-environment. However, the natural weathering process has the potential to be locally
99 exaggerated by any future mining of SMS deposits and exposure of significant fresh surface area.

100

101 The majority of previous dissolution studies are related to terrestrial acid mine drainage arising from mine flooding
102 and leaching of tailings piles by meteoric waters (Acero et al., 2009; Bonnissel-Gissingner et al., 1998; Constantin
103 and Chiriță, 2013; Descostes et al., 2004; Kwong et al., 2003; McKibben and Barnes, 1986; Moses et al., 1987). A
104 small number of dissolution studies of specific sulphide minerals in seawater have been undertaken (Bilenker,
105 2011; Bilenker et al., 2016; Feely et al., 1987; Romano, 2012) and demonstrate the large difference in oxidation
106 rates between different sulphide minerals, in particular, the two order of a magnitude difference in abiotic oxidation
107 rates between pyrrhotite and chalcopyrite. These rates quantitatively predict that any acid production from 'in situ'
108 mining of SMS deposits will be buffered by advecting seawater and that mine waste has the potential to persist on
109 the seafloor for years without complete oxidative transformation (Bilenker et al., 2016). However, these studies are
110 typically undertaken with relatively large grain size fractions > 45 μm and are representative of 'in situ'
111 mining/extraction rather than the potentially more impactful dewatering and return processes that involves grains <
112 8 μm . Furthermore, these studies do not take into consideration any potential galvanic effects that may occur within
113 a natural SMS ore that contains a range of co-existing sulphide minerals. A galvanic cell occurs where two
114 different sulphide minerals are touching in the presence of an electrolyte such as seawater. The mineral with the
115 lower resting potential behaves as an anode and preferentially dissolves, protecting the other mineral which is
116 behaving as a cathode (Fig 1; Mehta and Murr (1983)). As highlighted by Heidel et al. (2013), pyrite in contact with
117 most common SMS sulphide minerals should be galvanically protected as a result of a high rest potential
118 compared to the other most common sulphides (Fig. 1). Within a seafloor context (higher pH's), this is similarly
119 expected to be the case; where even though rest potentials are lower, the relative difference of rest potential
120 between the minerals is constant. Galvanic cells have already been shown to increase dissolution and explain
121 observations within the context of terrestrial sulphide ore deposits (Abraitis et al., 2004a; Heidel et al., 2013; Koski
122 et al., 2008; Kwong et al., 2003; Li et al., 2006; Liu et al., 2008) and have also been put forward to explain
123 observations of the mineralogy of oxidised SMS deposits (Webber et al., 2015). Whilst not attributed to galvanic

124 cells, (Edwards et al., 2003) demonstrated that a mixed sulphide ore is notably more reactive on the seafloor than
125 individual sulphide minerals, albeit in the presence of bacteria.

126
127 SMS deposits are comprised of a variety of mineral grains, each often containing various inclusions, and it is the
128 galvanic interaction of these phases that may have the ability to substantially increase dissolution rates. The only
129 leaching study that simulates natural mixed sulphide rich sediments in seawater was undertaken as a result of
130 prospecting and a regulatory need to provide an environmental impact statement (EIS) for mining the Solwara-1
131 Deposit, Bismark Sea, Papua New Guinea (Gwyther, 2008). There are two parts to that study, the first undertaken
132 by Australia's Commonwealth Scientific and Industrial Research Organisation (CSIRO) (Simpson et al., 2007), the
133 second undertaken by Charles Darwin University (Parry, 2008). Whilst extensive leaching of a range of metals is
134 observed, the mineralogy of the ore used in experiments is not documented and only the bulk chemistry of the
135 ores is available (as reported in Supplementary Material A).

136
137 There is clearly a need for further studies that attempt to reproduce the true compositional range of the
138 materials that will be dispersed into the water column as a result of deep sea mining in a colder, deeper (high
139 pressure) more saline, and alkaline aqueous medium. This suspended particulate will include a variety of
140 minerals; many of which will have interfaces (or inclusions) that could lead to galvanic cells. These have the ability
141 to substantially increase the leaching of metals into the water column (Abratis et al., 2004b; Heidele et al., 2013;
142 Koleini et al., 2010; Kwong et al., 2003; Li et al., 2006; Liu et al., 2008; Majuste et al., 2012; Mehta and Murr, 1983;
143 Subrahmanyam and Forssberg, 1993). There are a multitude of variables to consider in this process including
144 mineralogy, bulk elemental chemistry, grain size distribution and surface area of the particles, pH, temperature,
145 pressure, salinity, dissolved oxygen and prevailing ocean currents. Mineralogy and geochemistry varies
146 considerably across sulphide ore deposits (Cherkashev et al., 2013; Hannington et al., 2005) as a result of factors
147 including tectonic setting (influencing the composition of the host rock), pressure, pH and temperature. As a result
148 of this, different extant ore deposits are expected to be oxidising and releasing a variety of different metals into the
149 oceans, all at different rates.

150
151 In this study, we begin to evaluate the potential for anthropogenic leaching of SMS ore as a result of future
152 seafloor mining. The important questions are: Whether leaching occurs and to what extent; Are certain deposits
153 more of an environmental risk to mine and require greater dilutions to meet toxicity guidelines; How will mineralogy

154 and geochemistry play a role in this process. To address some of these questions we have performed a series of
155 leaching experiments that investigate some of these variables for the TAG deposit. In particular, the selected
156 samples represent the diverse mineralogy from within this single ore deposit.

157

158 Three terms are used within this study to refer to the different processes occurring during leaching. **Leaching** is
159 the total loss of mineral solutes by the action of a liquid (seawater). In this context, the loss of minerals (sulphides)
160 is a result of their oxidative dissolution in seawater. The total amount of metals leached (lost) is not necessarily
161 **dissolved** in the subsequent leachate (seawater) due to the **precipitation** of Fe oxide/oxy-hydroxides and
162 sequestration of metals onto oxides. The term **dissolved** refers to the metals remaining in the seawater (after
163 filtration and removal of oxides).

164 **2 Materials**

165 Samples from the TAG deposits, Mid-Atlantic Ridge (MAR) were supplied through the Integrated Ocean Drilling
166 Program (IODP). Cores were recovered from five sites along the TAG hydrothermal mound (Fig. 2) during Leg 158
167 of the IODP between October and November 1994 (Humphris et al., 1996, 1995). The five areas are named TAG-
168 1 to TAG-5, where TAG-1 is located closest to the centre of the mound, approximately 20 metres SE of the black
169 smoker complex. 3 TAG samples were chosen for experiments as a result of their range in mineralogy as well as
170 availability of material. TAG samples H and J are taken from TAG-4 area, west of the central black smoker
171 complex and TAG B is taken from TAG-3, SW of the Kremlin area (Fig. 2).

172

173 An aliquot of each TAG sample was cut, mounted in epoxy and polished as a block for characterisation of the
174 whole rock sample. The remainder was crushed using a pestle and mortar and dry sieved to a size of <45 µm.

175

176 To ensure that any observed heavy metal leaching is a true reflection of the surface area with clean surface (as
177 though freshly mined) and to control grain size, all fine sulphide and oxide particles (<2.5 µm) were removed. As a
178 result of mixed sulphide ores being used in experiments and the high solubility of sphalerite and galena at low pH
179 (Abratis et al., 2004b; Heidel et al., 2013; Malmström and Collin, 2004; Weisener et al., 2004), a cleaning method
180 was adopted from Romano (2012). The cleaning method included 5 minutes of ultra sonication in acetone, a 5
181 minute ethanol rinse through 2.5 µm filter paper, drying in a desiccator, agitation in 1M HCl for 30 seconds

182 followed by a 5 minute soak, with a final ethanol rinse through 2.5 μm filter paper before drying in a vacuum
183 desiccator.

184

185 This cleaned 2.5 - 45 μm size fraction was always stored at room temperature in a vacuum desiccator to prevent
186 oxidation, and individual aliquots were removed for characterisation and leaching experiments.

187 **3 Characterisation**

188 TAG samples were characterised as polished blocks as well as cleaned powders prior to leaching experiments.
189 Unfortunately, it should be noted that reacted sulphide material (and any oxide phases that had formed during the
190 experiment) was not retrieved or analysed posterior to experiments as it proved too fine to identify individual oxide
191 particles for characterisation and too small in volume for powder X-Ray diffraction (XRD) analyses.

192 **3.1 Sulphide ore Blocks**

193 Polished blocks of each sample were examined by reflected light microscopy to identify the major ore minerals and
194 subsequent scanning electron microscopy (SEM) with an energy-dispersive X-ray (EDX) detector for further
195 identification of phases and their semi-quantitative elemental compositions. The SEM instrument used was a Carl
196 Zeiss SigmaTM variable pressure SEM with a GeminiTM field emission electron column with Octane-PlusTM
197 silicon drift detector. The instrument utilises TEAM analytical software from EDAX. Table 1 provides a summary of
198 the phases identified, their abundances (wt %), textures and the inclusions observed. Representative reflected
199 light photographs of each sample along with SEM backscattered images are shown in Fig. 3.

200

201 In addition, some laser ablation-inductively coupled plasma-mass spectrometry (LA-ICP-MS) spot analysis (wt%
202 ppm) were collected on some Cu-poor phases (included in Table 2). This data was collected to help provide an
203 explanation of dissolution results as well as an indication of which minerals are likely to be dissolving. LA-ICP-MS
204 analyses were carried out using a Nu Instruments ATTOM HR-ICP-MS at GEOMAR, Helmholtz Centre for Ocean
205 Research, Kiel. For detailed methodology, please refer to Supplementary Material B.

206 **3.2 Sulphide ore powder**

207 Powder XRD was conducted using a Phillips X'Pert Pro diffractometer with a Cu $K\alpha$ source, detailed methodology
208 is outlined in Supplementary Material C. This provided an overall representation of the phases present including

209 semi-quantitative analysis presented in Table 1 with individual XRD patterns shown in Supplementary Material C1.
210 An aliquot of each cleaned sulphide powder was mounted in resin and polished to 1 μm diamond grade. This
211 allowed for identification of mineralogy of individual grains and inclusions (Fig. 4). Bulk Fe and Cu data of all
212 powder samples are also presented in Table 1. Samples underwent aqua regia digestion, with arising solutions
213 analysed on an SPECTRO Ciros SOP inductively coupled plasma - optical emission spectrometer (ICP-OES) at
214 the University of Kiel, Germany. For a more detailed methodology, please refer to Supplementary Material D. As
215 there is the potential for a wide distribution of grain sizes in between the resulting 2.5 – 45 μm size fraction of
216 sulphide powders, surface area analysis was undertaken to highlight any differences between samples (due to
217 grain size and/or mineralogy) and allows for normalisation of results. The surface area of all cleaned size fractions
218 were determined using the Brunauer, Emmett and Teller (BET) multiple point N_2 surface area method, on a
219 Quantachrome NOVA 1200 and are quoted in Table 1.

220 **4 Experimental Methods**

221 Seawater solutions were made according to the recipe of Millero (2013). They were found to contain on average
222 391.96 ± 27.66 ppb Fe, 172.63 ± 39.16 ppb Cu and 73.85 ± 19.41 ppb Pb as contaminants. Approximately 0.6 - 1 g
223 (dependent on availability) of natural TAG sulphide ore of 2.5 - 45 μm was added to 500 mL of seawater.
224 Conductivity, pH and dissolved oxygen (DO) readings were taken throughout the experiments using a HACH
225 meter. Conductivity was calibrated at 12.85 and 53.0 mS cm^{-1} and pH measurement was calibrated at 4.01 and 9.
226 All experiments were stirred using a magnetic flea, the rate of stirring was chosen so that particles remained
227 suspended, analogous to a dewatering of the ship-board ore in a mining context. Temperatures were held at
228 approximately 12 ± 1 $^\circ\text{C}$ (simulating the sea surface) using a refrigeration unit. Dissolved oxygen concentrations
229 were controlled by varying the ratio of compressed air to nitrogen using sintered flow meters and were held at
230 approximately 9.0 mg L^{-1} across the duration of each experiment. This oxygen concentration is representative of
231 concentrations within proximity of the TAG hydrothermal field, where values in the Atlantic (A05) eWoce database,
232 show a range between 8.2 and 8.856 mg L^{-1} with the highest concentration observed at 5 km depth at a
233 temperature of 1.5 $^\circ\text{C}$ (Schlitzer, 2000). Features of individual experimental runs are summarised in Table 3.
234
235 During each experimental run, trace amounts of sulphide material were lost onto the surfaces of monitoring probes
236 and during sample filtration. In order to account for this, the wastewater was filtered, desiccated and weighed, and
237 the value subtracted from the initial weight, as shown in Table 3.

238 4.1 Sampling protocol

239 Dissolution experiments adopted a semi-batch design, as described in Rimstidt and Newcomb (1993) and Salmon
240 and Malmström (2006). Seawater samples (13 mL for metal analysis) were removed using a 10 mL mechanical
241 pipette (with an error of 0.5%) for analyses. 13 mL of fresh seawater is added to replace the volume lost at each
242 sampling interval (total of 156 mL over the course of each experiment), with any resultant dilution corrected for
243 (see Section 4.3).

244

245 Removed batch samples were filtered using a 0.22 µm pore size to remove all sulphide material and halt any
246 further reaction. Sampling occurred every 10 minutes for the first hour, every half an hour for the following two
247 hours and every hour up to the full 5 hours run time. 5 hours run time was chosen to be representative of the
248 amount of time it would take for a steady state to occur between the sulphide and seawater and also reflects the
249 period of agitation related to SMS mining.

250

251 Extracted aliquots were analysed using an Agilent 710 ICP-OES. Filtered (0.22 µm) solutions were acidified with
252 2% HNO₃ in a 2:1 ratio (3 mL sample to 6 mL of nitric acid) to prevent metals from precipitating out and to lower
253 the total dissolved solids to <1%. All samples were analysed for Fe (234.350), Cu (327.395), and Pb (220.353)
254 with chosen emission lines in brackets. Units of measurement are µg/L, referred to here as ppb. Standards for
255 metals ranged from 1-10 ppm. Limits of detection for the ICP-OES for Fe, Cu, and Pb are 0.70, 1.22, and 6.52 ppb
256 respectively.

257 4.2 Corrections

258 To account for 13 mL of sample removal and subsequent dilution with 13 mL of fresh seawater, the equations of
259 Salmon and Malmström (2006) were used (Eq. 5). This calculation assumes that elements measured in previous
260 samples remain in solution. The accumulated amount, N , of element j remaining in solution up to sample k ,
261 calculated from the measured concentration, C_{meas} , is determined by:

262

263 Equation 5

$$264 N_{k,j} = \left[C_{k,j,meas} (V_{0,total} - V_{k,ret}) + \sum_{s=1}^k C_{k,j,meas} V_{s,sample} \right]$$

265

266 All analysed solutions were also corrected for the dilution with nitric acid and initial seawater composition (including
267 removing seawater starting concentrations of Fe, Cu and Pb). These 'corrected' concentrations will henceforth be
268 referred to as 'measured' concentrations.

269

270 Measured concentrations were subsequently combined with other data (mass, surface area) in order to highlight
271 the implications for SMS mining. To identify the effect that bulk chemistry and different mineral mixtures (and
272 galvanic effects) exerted on leaching and metals observed in solution, absolute measured concentrations (ppb)
273 require a correction for the variability of sample mass used in each experiment. This correction is outlined in Eq. 1
274 in Supplementary Material E. To assess the potential metal leaching during mining scenarios, absolute measured
275 concentrations (ppb) require a series of corrections including 1) conversion to μmol 2) correction for volume of
276 seawater used and 3) a correction for the sample mass and surface area. These correction procedures are
277 outlined in Eq. 2 and Eq. 3 in Supplementary Material E. In this way, results can be extrapolated for leaching
278 outside of the fixed rock to fluid ratio (g/L) using here.

279 **5 Results**

280 Actual measured concentrations and errors (ppb), without corrections for surface area, mass of ore and volume of
281 seawater are presented in Supplementary Material F1. However to compare between different samples it is more
282 informative to correct these values to reflect the mass (g) of ore used (Section 5.1) as well as the different
283 available reactive surface areas (Section 5.1)

284 **5.1 Concentrations corrected for mass, volume and surface area ($\mu\text{mol}/\text{m}^2$)**

285 Measured concentrations and errors (ppb) converted to μmol and corrected for surface area, volume of seawater
286 and mass of ore used are presented in Figure 5, using data produced in Supplementary Material F2. Shown for
287 reference are representative maximum solubility's of Cu, Fe and Pb in seawater taken from experimental and
288 calculation studies (Angel et al., 2015; Franklin et al., 2001; Liu and Millero, 2002). As noted in Figure 5 and
289 discussed in Section 6, all elements (but particular Fe) may show an increase in the seawater as the metal is
290 leached and/or a decrease as the metal is removed from solution by precipitation of or absorption onto an oxide.

291 5.1.1 Cu

292 All samples show an initial rapid leach of Cu producing a concentration peak measured at the beginning of each
293 experiment but differing in magnitude and time between samples. The maximum concentration peaks for Cu are
294 up to: 3.89 ± 0.07 , 0.47 ± 0.26 and 2.37 ± 0.09 $\mu\text{mol}/\text{m}^2$ for TAG-B, H, and J respectively. This initial leach then drops
295 significantly and remains at a more consistent level. After 30 minutes, the average dissolved Cu was 0.09 ± 0.018 , -
296 0.04 ± 0.33 and 2.41 ± 0.06 $\mu\text{mol}/\text{m}^2$ for TAG-B, H and J. Whilst these are average values, the experiment with TAG-
297 B shows a subsequent slow decrease in aqueous Cu down to 0.01 ± 0.01 (~ 0 within error). This is in contrast to the
298 experiment with TAG-H where there is overall negligible change in Cu, with only spikes of 0.27 ± 0.28 and
299 0.41 ± 0.37 $\mu\text{mol}/\text{m}^2$ that are within error of 0 and 0.04 $\mu\text{mol}/\text{m}^2$ respectively. TAG-J is the only experiment where
300 there is an initial leaching of Cu that does not decrease to 0 throughout the 300-minute sampling window. Within
301 this average of 2.37 ± 0.06 , there is a peak of 2.69 ± 0.06 $\mu\text{mol}/\text{m}^2$. From the 90 minute sampling interval onwards,
302 the amount of Cu dissolved decreases from this peak value but only down to 2.04 ± 0.06 $\mu\text{mol}/\text{m}^2$.

303 5.1.2 Fe

304 All samples show an initial leach of Fe to the seawater producing a peak at the beginning of each experiment similar
305 to the observed behaviour of Cu, except here Fe concentrations exceed the solubility limit of seawater. Again,
306 similar to the Cu peak, the magnitude of the Fe peak differs between samples. The initial peaks of Fe are
307 1.63 ± 0.04 , 0.47 ± 0.19 and 0.54 ± 0.12 $\mu\text{mol}/\text{m}^2$ for TAG-B, H and J respectively. This initial dissolved concentration
308 then drops to negative Fe values after the 20-minute sampling interval for experiments with TAG-B and TAG-H
309 and after the 90-minute sampling interval with TAG-J. At the 120-minute sampling interval, TAG-H displays a spike
310 in Fe concentration at 0.99 ± 0.19 $\mu\text{mol}/\text{m}^2$ which does not correspond to either of the Cu spikes of the same
311 experiment. The fall to negative values (below initial seawater background) is consistent with the precipitation of Fe
312 oxides and exceedance of the solubility limit of Fe in seawater.

313 5.1.3 Pb

314 Whilst there is an initial leaching of Pb in experiments with TAG-H and TAG-J, in contrast to the behaviour of Cu
315 and Fe in the same experiments, the initial dissolved Pb is comparable to later sampling intervals. The initial peaks
316 of Pb are 0.18 ± 0.16 and 0.20 ± 0.13 $\mu\text{mol}/\text{m}^2$ for TAG-H and J respectively. TAG-B shows negligible leaching
317 initially and throughout the experiment with the exception of small spikes at the 20 and 90-minute sampling
318 interval, which are within error of 0.

319

320 TAG-H and TAG-J show consistent net dissolved Pb throughout the entirety of the experiments. Whilst there are
321 fluctuations during each experiment, there is no overall increase or decrease in the dissolved concentrations of Pb.
322 Across the whole experiment there is an average dissolved concentration of $0.17 \pm 0.16 \mu\text{mol}/\text{m}^2$ and 0.16 ± 0.11
323 $\mu\text{mol}/\text{m}^2$ of Pb for TAG-H and TAG-J respectively. However, the maximum Pb dissolved throughout the 300
324 minute-sampling interval is $0.38 \pm 0.12 \mu\text{mol}/\text{m}^2$ versus $0.27 \pm 0.08 \mu\text{mol}/\text{m}^2$ for TAG-H and TAG-J respectively.

325 **5.2 Concentrations corrected for mass (ppb / g)**

326 Results presented in $\mu\text{mol}/\text{m}^2$ cannot be used to directly infer the effects of mineral mixtures, as the surface area of
327 the ore used within the correction for each sample is a summation of the surface area of multiple different mineral
328 phases. Instead, measured concentrations and errors (ppb) corrected for grams of ore used in each experiment
329 are presented in Figure 6. Data are presented in Supplementary Material F3. Furthermore, data presented in this
330 way can provide an idea of the actual magnitude of dissolved metals when scaled up to ore production quantities.

331

332 TAG-J shows the highest dissolved concentration of metals in seawater, on average (from the 30 minute sampling
333 interval) 186.01 ± 4.96 ppb Cu per gram of ore and 39.45 ± 26.54 ppb Pb per gram of ore. TAG-H shows similar
334 concentrations of Pb to TAG-J, with an average of 42.78 ± 37.74 ppb per gram of ore after the 30-minute sampling
335 interval.

336 **6 Discussion**

337 Seafloor SMS material that is disturbed during in situ mining, along with fine particulate SMS materials returned to
338 the ocean after surface processing will initially be suspended in the water column as a sediment plume and may
339 be dispersed into the wider ocean, but will ultimately settle out onto the seafloor. Whilst there is still the potential
340 for toxicity and leaching, the in situ extraction is argued to pose less of a risk as a result of the larger grain sizes of
341 the arising particulates (less surface area available for leaching as well as a quicker settling rate, reducing the time
342 the sulphide is exposed for leaching) (Gwyther, 2008). In particular, a study by Bilenker et al. (2016) suggests that
343 acid generation during in situ mining is slow and unlikely to be problematic.

344

345 Leaching experiments presented in this study are most representative of the dewatering process during ship-board
346 processing and return of material to the sea, where finer particles are exposed to seawater. During exposure there

347 is potential for these fine sulphide particles to experience more substantial dissolution and release of heavy
348 metals, both locally or some distance into the open sea. Quantification of the distal extent of such plumes and
349 subsequent leaching is difficult to speculate upon without modelling of site-specific plume generation. To this end,
350 stochastic hydrodynamic modelling from Gilbert et al. (2008) was used to investigate the impact of discharging
351 return water at Solwara 1, and the results are applicable to experiments here. The modelling involved a range of
352 variables (dilution rates, temperatures) and found that plumes would dissipate and achieve a dilution of 5000 times
353 within 0.6 km from the point of discharge. The estimated maximum sub-sea plume thickness within the water
354 column is 175 m.

355

356 Whilst the Gilbert et al. (2008) model demonstrates that the concentration of fine material ($<8 \mu\text{m}$) dilutes fairly
357 rapidly with distal extent, the time it will take for it to fall to the seafloor (and out of the water column) from the
358 designated 25 to 50 m height above the seafloor is not stated. During this time, it will be exposed to seawater,
359 allowing leaching to progress. Experiments in this study demonstrate the early dissolution of metals, with high-
360 resolution time steps. Gilbert et al. (2008) state that over the lifetime of the mining operation (20 months), the peak
361 bottom thickness from the settling fine material is less than 0.1 mm. Based on assumptions made in the modelling
362 as applied to the EIS and using Stokes Law, an $8 \mu\text{m}$ pyrite particle (density of 5 g/cm^3) would take 1.87 days to
363 settle out from a height of 50 m. However, a $0.1 \mu\text{m}$ pyrite particle, would take 12010 days to settle from a 50 m
364 height above the seafloor. Without a better understanding of the grain size distribution within the $<8 \mu\text{m}$ size
365 bracket, it is difficult to quantify the amount of time sulphide material will ultimately persist and leach in the water
366 column. Furthermore, even after any fine material has settled, whilst the surface area exposed has been reduced,
367 there is still potential for further leaching of metals as the material lies as a poorly consolidated seafloor deposit.

368

369 The experiments of this study simulate the consistent stirring of sediments and as a result, the ore has the
370 maximum exposure for leaching. This is representative of the early leaching process that will occur prior to settling
371 or dilution, especially in the finer fraction.

372

373 Within the first 10 minutes, all samples show initial dissolved concentrations of Cu and Fe, at varying magnitudes
374 (Fig. 5). Fig. 7 demonstrates the average dissolved metal as a proportion of the bulk concentration, expressed as a
375 percentage. Whilst percentage dissolved values are in themselves small, it is important to note the high bulk
376 concentrations of heavy metals in the TAG samples; making this small loss significant in terms of toxicity. TAG-H

377 demonstrates the highest initial percentage loss of Cu and Pb, whilst TAG-B shows a high loss of Cu and TAG-J a
378 loss of Pb.

379

380 Using the data of this study as a 'realistic' example (although this ignores any abiotic contribution), these results
381 suggest that a total of 0.04 and 0.002 wt% of Cu, Fe and Pb will be leached from a deposit such as TAG-H and
382 TAG-B respectively, at the initial stages of processing (Fig. 7). However, with removal of both Cu and Fe from
383 solution by oxide precipitation after 10 minutes (based on exceedance of solubility limit and observation), this
384 effect is reduced even more dilution subsequently occurs.

385

386 A deposit such as TAG-J is more concerning. 0.03 wt% of Cu, Fe and Pb will be lost in the initial stages of
387 processing (Fig. 7a), but leaching of Cu and Pb will continue (Fig. 7b) until either the particle interface has been
388 fully dissolved or an oxide forms on the particle surface and insulates it from the seawater (passivation on the
389 surface, which is expected in most cases). However, the fact that precipitation of oxides is not shown to remove
390 the dissolved metals for TAG-J is a cause for concern. In the TAG experiments where a loss is observed, Pb and
391 Cu have the highest percentage dissolved, indicating their higher propensity to be leached and stay in solution
392 compared to Fe. This is also observed in experiments undertaken in the EIS (see Fig. 7).

393

394 Sample TAG-J shows the only sustained dissolved concentrations of all the experiments in this study, with both
395 Cu and Pb present in seawater, remaining at a significant level (Fig. 5, 6 and 7). Whilst all three TAG samples
396 contain similar concentrations of Pb (100-200 ppm, Table 1), it is only TAG-H and TAG-J that show leaching of Pb
397 into seawater (both at ~ 40 ppb). TAG-B, a sample that contains a similar, if not higher, total amount of
398 chalcopyrite and bulk Cu as TAG-J (Table 1), shows initial leaching of Cu (Fig. 5), but this is removed after 30
399 minutes.

400

401 Due to the design of these experiments, precipitations of metal oxides are guaranteed under these high pH
402 conditions in all experiments, mainly precipitating Fe-oxide, but also having the potential to sequester and remove
403 Cu and Pb. All were run at similar oxygen concentrations where oxygen was never limited and kept constant
404 throughout, ensuring the formation of oxide precipitates throughout the course of experiments, (Table 3), yet both
405 TAG-J and TAG-H have sustained dissolved metals that are not removed from solution. This indicates that the
406 leaching of Cu from TAG-J is at a higher magnitude than any removal through oxidation (due to mineralogy or

407 galvanic effects) and that the method of removal of Cu and Pb from TAG-B is different to TAG-J and TAG-H (due
408 to mineralogy). This is discussed further in Section 6.1. Either way, the leaching results demonstrate that bulk
409 chemistry does not dictate the concentration of metals dissolved into seawater. Instead, mineralogy and/or
410 possible galvanic effects are the driving forces behind the type and concentration of metals remaining in seawater
411 after leaching.

412

413 As shown in Fig. 6a, b and c, the high concentrations of Fe and Cu dissolved in experiment TAG-J are very similar
414 to those observed in experiments from the EIS. The figure shows results from two different published experimental
415 datasets that have the most similar run conditions to those used in the current study. The specific mineralogy of
416 the samples used within the EIS was not presented for either the experiments of Parry (2008) or Simpson et al.
417 (2007), although the overall chemistry was provided and is reproduced in Supplementary Material A. Based on this
418 chemistry, the mineralogy is substantially different between each of their experiments.

419

420 Data from Parry (2008) uses predominantly Fe-rich samples (31.6 % Fe, 5.13 % Cu, 3670 ppm Zn) similar to our
421 experiments with deposits from TAG (Table 1, bulk Fe and Cu) with Cu and Pb dissolved at similar concentrations
422 as TAG-J, despite a larger grain size, and higher temperature and rock-fluid ratio. Studies by Moses and Herman
423 (1991) and Simpson et al. (2007) indicate a linear relationship between rock to fluid ratio and dissolved metals,
424 allowing for data to be scaled to take into consideration the difference in rock-fluid ratio between studies. When
425 data from Parry (2008) is scaled to the rock-fluid ratio used in this study (2 g/L), concentrations drop to ~3 ppb for
426 Cu and ~2 ppb for Pb. This lower concentration/lower percentage loss of bulk observed in the EIS data when
427 scaled to 2 g/L (Fig. 6 & 7) can be explained by the larger grain size (less surface area) used in experiments.

428

429 The ore used in experiments by Simpson et al. (2007) has significantly higher bulk Cu, Zn, Pb and As than ore
430 used by Parry (2008) and the TAG samples used here (Supplementary Material A). Despite this, the dissolved Cu
431 and Pb is much lower than the comparable experiments with Fe-rich ore as shown in Fig. 7. This is comparable to
432 our results, where bulk chemistry does not define the metals that are leached and remain in solution. What is not
433 shown in this figure, is the high dissolved concentrations of Zn and As during the EIS experiment with the Cu-Zn-
434 Pb rich ore (Supplementary Material A). This could imply a preferential dissolution of Zn and As rich minerals (e.g.
435 sphalerite and arsenopyrite/As sulfosalts) over Cu and Fe, suggesting either galvanic cells are at play or that the
436 dissolution rate of Zn and As bearing minerals is quicker.

437

438 Based on the effect differing mineralogy has on the leaching of SMS ores presented in this study, it is imperative
439 that extensive tests with the full range of mineralogy and geochemistry of ore mined are undertaken prior to any
440 future mining of a deposit. Results where only one type of ore are utilised in experiments are applicable to only a
441 particular area of a deposit and are not ubiquitously transferable.

442 **6.1 The effect of mineralogy on leaching and dissolved metals**

443 By combining the observed mineral proportions and bulk chemistry from Table 1 with the magnitude of metal
444 released to the seawater (ppb), corrected for grams of ore tested (Fig. 6), it should be possible to at least
445 speculate on the effect that mineralogy, texture and possible galvanic reactions might have on the 'leaching'
446 process. It must be remembered that the 'leaching' simulated here and in particular the monitoring of metal release
447 with time as sulphide dissolves, will be counteracted by subsequent oxide precipitation in these experiments. The
448 measured metals in solution can only give a net view of the two competing processes. The dissolved oxygen levels
449 in the seawater have been fixed at a value that is representative of the TAG field in these experiments (Schlitzer,
450 2000) although this could be a local variable. Fe is the major contributor to the precipitate (due to its low solubility
451 in seawater), forming Fe oxides/oxy-hydroxides. The 'absorption' of other heavy metals (e.g. Cu, Pb) onto Fe
452 oxides and oxy-hydroxides has been extensively demonstrated in the literature (Benjamin and Leckie, 1981;
453 Davranche and Bollinger, 2000; Grybos et al., 2007; Jong and Parry, 2004; Liu and Huang, 2003). Absorption of
454 trace metals onto (and subsequently into) iron oxides and oxy-hydroxides is observed to be rapid, on the time
455 scale of hours, (Ahmad et al., 2012; Balistrieri and Murray, 1982) so it likely to be an important process on the
456 timescale of this study as well as the actual mining operation. It is unfortunate that design of the current study
457 produces too small an amount of precipitate to collect and measure the trace metal composition.

458

459 In addition to the new Fe-oxide precipitation, some ore samples such as TAG-B initially contain a high proportion
460 of Fe oxides and oxy-hydroxides (Fig. 3, Table 1) that would represent a large surface area of the processed ore
461 material, and will be present at the beginning of our leaching experiments. This could represent either a source to
462 release metals or remove them in a similar way to the newly formed Fe precipitate. In the latter case, the presence
463 of Fe oxides/oxy-hydroxides within the deposit prior to mining (likely in the case of an inactive SMS deposit) could
464 be advantageous in reducing the environmental toxicity associated with mining.

465

466 Samples have all been crushed and sieved to the same grain size fraction (2.5 to 45 μm) to remove this as a
467 variable between experiments. Whilst there is the potential a range of distributions within this size fraction, this
468 potential should be eliminated during the normalisation of the data to the surface area of each specific sample (Fig.
469 5).

470

471 All samples here show an initial increase in Fe, which is undoubtedly caused by sulphide ore dissolution. This is
472 followed by a rapid decrease to background levels in a few hours, although TAG-B and H fall more rapidly than
473 TAG-J. The solutions are observed to fall below the original background seawater levels (Fig. 5 and 6), indicating
474 that in some cases the original seawater Fe is removed from solution (oxidised) also. The dissolved oxygen
475 concentration is kept constant throughout the experiment, ensuring they are never oxygen limited and it is possible
476 to continuously form oxides as would be expected in the natural environment. The fall in Fe is either due to a one
477 off initial release and subsequent precipitation of Fe as an oxide with time, or an increase in the precipitation rate
478 over the continuous release rate.

479

480 All three TAG samples contain similar Pb concentrations (100-200 ppm), yet only samples TAG-H and J show
481 leaching. No galena or major Pb bearing minerals were identified in the samples, indicating that the Pb must arise
482 from the lattice sites of sulphide phases (Table 2), though it is not possible to identify the particular mineral phase
483 contributing the Pb from this data alone. The observation that TAG-B has negligible Pb dissolved whilst
484 demonstrating similar bulk Pb suggests that Pb is present as a phase that is not leaching or more stable (e.g.
485 sorbed onto present Fe oxy-hydroxide).

486

487 Based on bulk analysis alone (Table 1), it might be expected that TAG-B would demonstrate the highest Cu
488 release and concentration in the seawater. Whilst it does leach the highest initial concentration of Cu (Fig. 5), it is
489 TAG-J that maintains the higher dissolved Cu throughout the 300-minute experiment. It is clear from the TAG-J
490 experiment that the formation of oxides does not keep up with the leaching of Cu, resulting in consistently high
491 dissolved Cu. The disparity between TAG-B and J can ultimately be explained by either 1) a different Cu
492 host/source, 2) a difference in mechanism leaching Cu, 3) a difference in mechanism removing Cu or 4) a
493 difference in exhaustion/isolation (passivation) of Cu host/source. These possibilities are discussed in further detail
494 below.

495 6.1.1 *Hosts and sources of Cu*

496 Chalcopyrite is the largest source of Cu observed in both TAG-B and TAG-J (6.2 and 5.6 wt% respectively). In
497 reality, chalcopyrite has been shown to have at least an order of a magnitude slower dissolution rate than both
498 pyrite and marcasite (Bilenker, 2011; Feely et al., 1987; Romano, 2012). As a consequence of this, a sample such
499 as TAG-H (~42% marcasite) or TAG-J (83.8% pyrite) might be expected to dissolve the fastest and not only leach
500 the most Fe, but also a certain amount of Cu, which is present at trace levels in the mineral lattice (see Table 2).
501 This then could become a more important source of Cu than the major host chalcopyrite. On closer inspection,
502 marcasite can be ruled out on the basis of two pieces of evidence: 1) low concentrations of Cu in its lattice (77.20
503 ppm, Table 2) and 2) TAG-H has a dominant marcasite mineralogy (~42%) with similar concentrations of Cu in its
504 lattice to TAG-J (70.75 ppm) but shows no significant release of Cu (Fig. 5).

505
506 The role of pyrite can also be assessed. As shown in Table 2, the TAG-J pyrite contains higher concentrations of
507 Cu in its lattice (715.30 ppm) than the pyrite in TAG-B (461.20 ppm). As TAG-J also contains 1.5 times more pyrite
508 than TAG-B, it might appear to be a plausible source of Cu during the leaching of TAG-J. However, with high
509 concentrations of pyrite (24.4 wt%) and high Cu in its lattice, it would be expected that TAG-B would also display
510 consistent dissolved concentrations of Cu if pyrite breakdown were the main Cu release mechanism and
511 proceeded at the same rate in both samples. Furthermore, if pyrite were the source in both, it would be expected
512 that TAG-J would have an initial higher leach than TAG-B, which is not observed. Based on these observations, it
513 is difficult to appeal to pyrite (or marcasite) as the source of released Cu.

514
515 Another plausible Cu source to consider and explain the disparity between TAG-J and TAG-B, would be secondary
516 formed Cu minerals. They have been demonstrated to have higher dissolution rates than chalcopyrite, but how this
517 rate compares to pyrite and marcasite is unknown (Fullston et al., 1999). TAG-J was shown to contain rare
518 covellite (CuS) during reflected light microscopy and XRD analysis at ~1.4 wt%. The leaching of covellite could
519 provide a tenuous explanation for the heightened dissolved Cu in TAG-J over TAG-B, but still does not explain the
520 higher initial leach of Cu during the TAG-B experiment.

521
522 The observation of dissolved Cu decreasing throughout the experiment with TAG-B could suggest exhaustion of a
523 Cu source or its isolation from the seawater. However, it would be difficult to explain why any reduction in
524 availability is occurring throughout the experiment in TAG-B and not TAG-J based on the constant dissolved
525 oxygen concentrations. For example, if passivation on the surface of Cu sulphide minerals (due to the formation of

526 oxides) were to occur and reduce the availability of Cu, it would be expected in both TAG-B and TAG-J
527 experiments. Another phenomenon with the potential to explain the disparity in dissolved Cu over time between
528 TAG-J and TAG-B is absorption, discussed earlier.
529
530 TAG-B contains a high quantity of Fe-oxides and oxy-hydroxides (Fig. 3) that would be present during leaching.
531 Absorption of heavy metals onto Fe oxides and oxy-hydroxides could account for the subsequent drop in Cu over
532 time observed during the experiment with TAG-B (Fig. 5). New oxide phases that form throughout the TAG-J
533 experiment are unlikely to provide as high of a surface area for absorption as the already established oxides
534 present in TAG-B do. If this is the case, the presence of Fe oxides/oxy-hydroxides within the deposit prior to
535 mining (likely in the case of an inactive SMS deposit) could be advantageous in reducing the environmental impact
536 associated with mining.

537 6.1.2 Galvanic cells

538 Notwithstanding the presence of covellite or the process of absorption, dissolution rates of the major sulphide
539 minerals alone cannot explain the observations found in this study. In terms of alternative causal effects, galvanic
540 cells have been shown to significantly increase dissolution (Abraitis et al., 2004a; Heidel et al., 2013; Koski et al.,
541 2008; Kwong et al., 2003; Li et al., 2006; Liu et al., 2008).

542
543 Whilst it is unlikely that any separate grains would be able to stay in contact for long enough to create a cell in
544 these stirred experiments, individual particles composed of multiple sulphide phases can create a cell with
545 seawater. Both TAG-B and TAG-J commonly demonstrate the occurrence of sulphide inclusions in whole rock
546 samples and cleaned sulphide ore powders (some less than 1 μm) of chalcopyrite in pyrite/marcasite grains and
547 vice versa (see Fig. 3 and 4), allowing galvanic cells the ability to form during leaching experiments. In this
548 scenario, the lower potential of chalcopyrite (Fig. 1) would cause it to be preferentially dissolved relative to pyrite
549 (or marcasite), releasing Cu and some Fe into solution.

550
551 TAG-B has much less pyrite than TAG-J (24.4% vs. 84% pyrite plus 6% marcasite), and consequently, fewer
552 inclusions to allow for galvanic cells to occur. If galvanic cells were playing a role, it would be expected that both
553 TAG-B and TAG-J would display a leach of Cu, just at a higher magnitude in TAG-J, which is not observed in the
554 initial leach (TAG-B has a higher initial leach). However, this could be easily explained by an initial leach of

555 chalcopyrite in both that slows with time (producing the higher initial leach of Cu in TAG-B), with galvanic cells in
556 TAG-J producing the higher dissolved Cu concentrations observed later on.

557

558 Exact quantification of the extent to which galvanic coupling, and mineralogy (and any associated absorption) is
559 contributing to dissolution role is not possible within the scope of this study, simply because there are numerous
560 inseparable variables at play. Nonetheless their impact on the leaching of SMS ore needs to be considered and
561 accounted for in environmental impact predictions.

562 **6.2 Toxicity potential**

563 The toxicity induced by sulphide dissolution may have some detrimental impact on the environment around SMS
564 deposits and associated ecosystems, although this will ultimately be highly variable. It has been speculated that
565 any high concentrations of heavy metals that are leached or present in the plume will pose minimal risk to a faunal
566 system already adapted to active SMS deposits (Simpson et al., 2007; Gwyther, 2008; Parry, 2008; Sander and
567 Koschinsky, 2011). However the most distal 'background' fauna may not have developed such survival strategies.
568 Furthermore, if mining occurs at inactive SMS deposits where adaptation to toxicity is lower, the impact to this
569 specific ecosystem may be more significant; unless these ecosystems have a high recovery rate.

570

571 Initial high metal concentrations (within 10 minutes) are unlikely to cause serious problem for fauna as they are
572 quickly removed via precipitation of oxides, with suffocation from plumes a more serious concern in the initial
573 stages. Whilst the average percentage loss (Fig. 7) is very small across all metals and samples (<0.1%), the
574 sustained dissolved metals at a ppb level is still considered significant due to their exceedance of both Australian
575 and New Zealand water quality (ANZECC) and UK Marine Special Areas of Conservation (SAC) environmental
576 guidelines. It is difficult to apply these guidelines to black smoker environments, where background toxicant
577 concentrations vary significantly and the ecosystems are dramatically different to 'normal' marine ecosystems. In
578 fact, no guidelines exist for such environments. For purposes of discussion and to compare experiments
579 undertaken here with those undertaken in the EIS by Solwara-1, the minimum guideline for each metal has been
580 chosen (99% protection, ANZECC). Guidelines are 0.3 and 2.2 ppb for Cu and Pb respectively.

581

582 Based on the current mining concept outlined by Nautilus Minerals for their EIS, the return water will include solid
583 material <8 µm in diameter with an expected total dissolved solids (TDS) of 6.35 g/L (Gwyther, 2008) compared to

584 the 2 g/L of this study. When experiments in this study are scaled to the rock-fluid ratio outlined in the EIS
585 (Supplementary Material G), Cu concentrations observations in TAG-J would increase to an average of 590.6 ± 15.7
586 and Pb to 133.4 ± 84.8 ppb. TAG-H's Pb concentrations would increase to an average of 135.8 ± 119.8 ppb. These
587 are well above guidelines before dilution is taken into consideration.

588
589 Based on experiments with 2 g/L, TAG-J would require 620 times dilution to reduce Cu concentrations to within the
590 0.3 ppb ANZECC guideline. When scaled to the expected 6.35 g/L rock to fluid ratio, a 1968 times dilution would
591 be required during mining. For TAG-H at 2g/L, a 19.4 times dilution would be required to bring the Pb
592 concentration in line with the 2.2 ppb UK-SAC guideline. This would increase to 61.7 times if scaling the
593 concentrations to the 6.35 g/L ratio. Elutriate experiments undertaken by Simpson et al. (2007) find that dilutions of
594 greater than 4000 times may be necessary for samples from Solwara, double the values suggested by this study.
595 The higher dilution requirement is likely to accommodate the high observed concentrations of As and Zn in their
596 dataset, elements which were not considered in this study. Whilst it is likely that As and Zn are present in higher
597 concentrations at Solwara than the TAG samples used here, data from Solwara experiments and trace element
598 studies (e.g. Hannington et al. (1991) and Wohlgemuth-Ueberwasser et al. (2015)) suggest that As, Zn, Co and Cd
599 could be leached during mining, and thus will require further investigation.

600
601 If the 2 g/L rock to fluid ratio is kept constant, localised toxicity would be expected in a stagnant water column.
602 However, in reality, dilution is expected where both plumes created by dewatering or extraction and deep-sea
603 currents have the ability to entrain fresh seawater. Hydrodynamic modelling can give an indication of dilution of
604 heavy metal concentration with distance but is site specific and does not take into consideration the time it would
605 take for dilution to occur. Gilbert et al. (2008) demonstrate a 600-fold volume dilution would be achieved within 85
606 m of the point of discharge at Solwara-1. However if TAG dissolved metal concentrations of this study were scaled
607 to 6.35 g/L, a 2000 fold volume dilution is required which would only be achieved at 600 m from the discharge.
608 Ultimately, the distance at which dilution is achieved to meet guidelines may not be sufficient, indicating either the
609 potential need for ship-board dilution prior to the return of waste water or refinement of the mining process. Of
610 more concern is that this does not include any ore particulate remaining in the diluted seawater volume, which may
611 continue to release further metals to solution during any dilution process.

612

613 In terms of total input into the ecosystem, the EIS for the proposed Solwara-1 deposit in Papua New Guinea
614 currently suggests a footprint of approximately 0.112 km² will be mined over five mineralised areas. If an area of
615 that size at TAG was to be mined and was identical in mineralogy, bulk chemistry and texture to TAG-J, there
616 would be a cumulative total of 0.224 moles of Cu (14230 ppm) added to the seawater throughout the mining
617 project.

618
619 Application of the data from this study and the Solwara-1 EIS might be 'conservative' if a finer ore size fraction (<8
620 µm) is taken into consideration. This could result in a significantly higher surface area and higher leaching rate.
621 The potential for toxicity during dewatering would be far more substantial than observed during the course of these
622 experiments. In addition, there are SMS deposits that are known to contain considerably higher concentrations of
623 toxic metals (As, Pb, Sb, Zn, Co, Cd, Ni and Hg) than TAG (e.g. mafic-hosted, felsic-hosted, young, back-arc basin
624 settings (Herzig and Hannington, 1995)), further increasing the potential for environmental impact.

625
626 Finally, it is widely accepted that Fe-oxidising bacteria play a significant role during the weathering (oxidative
627 dissolution) of seafloor sulphide ore deposits (Edwards et al., 2003). Rimstidt (1994), Plumlee et al. (1999),
628 Corkhill (2008) and Koski et al. (2008), all suggest that redox reactions utilising Fe³⁺ produced by bacteria catalyse
629 reaction rates of sphalerite, chalcopyrite, enargite and arsenopyrite. Lizama and Suzuki (1991), show that
630 *Thiobacillus ferrooxidans* and *Thiobacillus thiooxidans* both increase the leaching rates from sulphide minerals
631 (pyrite, chalcopyrite, sphalerite) by up to 44.2% in some cases. It has also been reported in numerous dissolution
632 studies (Ahonen et al., 1985; Berry et al., 1978; Jyothi et al., 1989; Mehta and Murr, 1983, 1982, Natarajan, 1988,
633 1985, Natarajan and Iwasaki, 1983, 1986; Yelloji Rao and Natarajan, 1989) that the presence of bacteria such as
634 *Thiobacillus ferrooxidans* in a polymetallic sulphide mixture can accelerate galvanic interactions significantly. Whilst
635 the role of microbes is highly important in the longer-term, in-situ, natural oxidation of seafloor sulphide ore
636 deposits, it has been suggested that abiotic oxidation rates of sulphide minerals are more relevant to the oxidation
637 of sulphides during seafloor mining (Bilenker et al., 2016; McBeth et al., 2011). It is postulated that bacterial
638 colonization of freshly ground mineral surfaces is unlikely under the rapid time spans of mining (<30 minutes based
639 on mining scenarios outlined by Nautilus Minerals Inc. However biotic oxidation could be of significant concern
640 once fine sulphide material has settled after initial extraction and dewatering. Leaching of metals has the potential
641 to continue after material has settled, not only abiotically but also when bacteria colonise the high surface area of
642 sulphide material that has been exposed due to mining.

643 **7 Conclusions and future directions**

644 Experiments presented here at 1 atm and 12°C with SMS ore samples from TAG, Mid Atlantic Ridge show a
645 dissolved concentration of metals (primarily Cu and Pb) at the parts per billion range that is not balanced by
646 oxidation and precipitation over time. Quantifying the extent to which factor such as galvanic coupling, and
647 mineralogy (and any associated absorption) or even biotic processes contribute to dissolution rates is not possible
648 within the design of this study, but will need to be assessed in future studies. Nonetheless, the results of this study
649 clearly demonstrate that the complexity surrounding the leaching of SMS ore needs to be considered and
650 accounted for in environmental impact predictions. A combination of this study with analysis of the precipitated
651 oxides would be a first step in advancing our understanding. It is also worth noting the higher pressure involved on
652 the seabed.
653

654
655 The evidence presented here clearly demonstrates that bulk chemistry alone cannot dictate the concentration of
656 metals leached into seawater. Instead, a combination of mineralogy, absorption processes and/or galvanic effects
657 must be considered as the primary driving forces behind the type and concentration of metals released and
658 removed into the water column during SMS mining. As a result, it is imperative that extensive tests with the full
659 range of ore mineralogy from future prospect sites are undertaken prior to activation of any extraction activities.
660 Results where only one type of ore are utilised in experiments are applicable to only a particular area of a deposit
661 and are not ubiquitous. Furthermore, the study highlights that the presence of Fe oxides/oxy-hydroxides within the
662 deposit prior to mining (likely in the case of an inactive SMS deposit) could be advantageous in reducing the
663 environmental toxicity associated with mining. The full contribution of galvanic coupling on the leaching of SMS ore
664 remains unclear and observation of dissolution and oxidation in situ using atomic force microscopy (AFM)
665 experiments could help to advance our understanding of galvanic couples between specific mineral combinations.
666

667 In these experimental simulations, dissolved concentrations exceed the 99% protection, ANZECC toxicity
668 guidelines by 620 times, and would imply the formation of localised toxicity in a stagnant water column. In reality
669 this concentration will most likely be rapidly diluted by the entrainment of fresh seawater as a result of plume
670 mixing (during the mining process) and/or deep ocean currents (site specific). Nevertheless, the distance at which
671 dilution is achieved to meet guidelines is unlikely to be sufficient, indicating either a potential need for ship-board
672 dilution prior to the return of waste water or a refinement of the mining process. Dilutions required to meet toxicity
673 guidelines (for Cu and Pb) when mining a deposit like TAG, are less than half of those required for a deposit like

674 Solwara 1 and imply that a deposit such as TAG could pose less of a risk to mine (in terms of leaching and toxicity)
675 than Solwara 1. However, it should be noted that concentrations will be much higher compared to these
676 experiments when scaled to more realistic rock-fluid ratios and a finer grain size (< 8 µm) as proposed for seafloor
677 mining scenarios.

678

679 SMS deposits that contain higher concentrations of Cu and Pb than TAG, as well as other heavy metals in higher
680 abundance (e.g. mafic-hosted and felsic-hosted (young, back-arc basin) settings (Herzig and Hannington, 1995))
681 signify an elevated risk of leaching when considering their environmental impact during the mining process
682 (smaller grain size and higher rock-fluid ratio). This study highlights the importance of further research to predict
683 and mitigate the effects of imminent SMS mining.

684

685 In order for deep-sea mining to take place in the future, the environmental impact of such an undertaking needs to
686 be fully understood and demonstrated. Experiments highlighted here and future planned experiments can help
687 refine the mining processes and minimise detrimental impacts by providing recommendation of grain size fractions
688 and rock-fluid ratios that can be adopted to reduce any risk of leaching and toxicity. Furthermore, certain types of
689 deposit or mineralogies can be identified as presenting more or less of a risk. This can ensure minimal leaching
690 of heavy metals and a reduction of environmental impact.

691 **8 Acknowledgements**

692 We would like to thank The Engineering and Physical Sciences Research Council (EPSRC) and Ascension
693 Holdings Ltd (AHL) for financially supporting this research. We would also like to thank IODP for kindly providing
694 TAG samples that allowed for this study to take place. A huge thanks to Sven Petersen and Matthias Frische who
695 provided considerable assistance with collection and processing of LA-ICP-MS data at GEOMAR Helmholtz-
696 Zentrum für Ozeanforschung, Kiel. Dieter Garbe-Schönberg and Ulrike Westernströer provided much help and
697 guidance with the digestion and analysis of the TAG samples at the University of Kiel.

698 **9 References**

699

- 700 (CLCS), C. on the L. of the C.S., 2016. Oceans and law of the sea, United Nations [WWW Document]. Submissions, through Secr. United Nations, to Comm. Limits
701 Cont. Shelf, Purs. to Artic. 76, paragraph 8, United Nations Conv. Law Sea 10 December 1982.
702 (ISA), I.S.A., 2016. Deep seabed minerals contractors [WWW Document]. Int. Seabed Auth.
703 Abraitis, P., Patrick, R.A.D., Kelsall, G.H., Vaughan, D.J., 2004a. Acid leaching and dissolution of major sulphide ore minerals: processes and galvanic effects in
704 complex systems. *Mineral. Mag.* 68, 343–351. doi:10.1180/0026461046820191
705 Abraitis, P., Patrick, R.A.D., Vaughan, D.J., 2004b. Variations in the compositional, textural and electrical properties of natural pyrite: a review. *Int. J. Miner.*
706 *Process.* 74, 41–59. doi:10.1016/j.minpro.2003.09.002
707 Acero, P., Cama, J., Ayora, C., Asta, M.P., 2009. Chalcopyrite dissolution rate law from pH 1 to 3. *Geol. Acta* 7, 389–397. doi:10.1344/105.000001444
708 Ahonen, L., Hiltunen, P., Tuovinen, O., 1985. The role of pyrrhotite and pyrite in the bacterial leaching of chalcopyrite ores, in: Branion, R.M.R., Ebner, H.G. (Eds.),

709 Fundamental and Applied Biohydrometallurgy. Amsterdam, pp. 13–22.

710 Angel, B.M., Apte, S.C., Batley, G.E., Raven, M.D., 2015. Lead solubility in seawater: an experimental study. doi:10.1071/EN15150

711 Berry, V.K., Murr, L.E., Hiskey, J.B., 1978. Galvanic interaction between chalcopyrite and pyrite during bacterial leaching of low-grade waste. Hydrometallurgy 3, 309–326. doi:10.1016/0304-386X(78)90036-1

712 Bilenker, L., 2011. Abiotic Oxidation Rate of Chalcopyrite in Seawater: Implications for Seafloor Mining. University of California Riverside.

713 Bilenker, L.D., Romano, G.Y., McKibben, M.A., 2016. Kinetics of sulfide mineral oxidation in seawater: Implications for acid generation during in situ mining of seafloor hydrothermal vent deposits. Appl. Geochemistry 75, 20–31. doi:10.1016/j.apgeochem.2016.10.010

715 Bonnissel-Gissingner, P., Alnot, M., Ehrhardt, J.-J., Behra, P., 1998. Surface Oxidation of Pyrite as a Function of pH. Environ. Sci. Technol. 32, 2839–2845. doi:10.1021/es980213c

717 Cheng, X., Iwasaki, I., 1992. Pulp Potential and Its Implications to Sulfide Flotation. Miner. Process. Extr. Metall. Rev. 11, 187–210. doi:10.1080/08827509208914206

719 Cherkashev, G.A., Ivanov, V.N., Bel'tenev, V.I., Lazareva, L.I., Rozhdestvenskaya, I.I., Samovarov, M.L., Poroshina, I.M., Sergeev, M.B., Stepanova, T. V., Dobretsova, I.G., Kuznetsov, V.Y., 2013. Massive sulfide ores of the northern equatorial Mid-Atlantic Ridge. Oceanology 53, 607–619. doi:10.1134/S0001437013050032

722 Constantin, C.A., Chiriță, P., 2013. Oxidative dissolution of pyrite in acidic media. J. Appl. Electrochem. 43, 659–666. doi:10.1007/s10800-013-0557-y

724 Corkhill, C.L., 2008. The mineralogical and biogeochemical transformations associated with As-bearing sulphide minerals in acid mine drainage system. The University of Manchester.

725 Descostes, M., Vitorge, P., Beaucaire, C., 2004. Pyrite dissolution in acidic media. Geochim. Cosmochim. Acta 68, 4559–4569. doi:10.1016/j.gca.2004.04.012

726 ECORYS, 2014. Study to investigate state of knowledge of deep sea mining: Final report: Annex 5 Ongoing and planned activity.

727 Edwards, K.J., 2004a. Special Paper 379: Sulfur Biogeochemistry - Past and Present, Geological Society of America Special Papers. Geological Society of America. doi:10.1130/0-8137-2379-5

728 Edwards, K.J., 2004b. Formation and degradation of seafloor hydrothermal sulphide deposits. Geol. Soc. Am. Spec. Pap. 379, 83–96. doi:10.1130/0-8137-2379-5.83

730 Edwards, K.J., McCollom, T.M., Konishi, H., Buseck, P.R., 2003. Seafloor bioalteration of sulfide minerals: results from in situ incubation studies. Geochim. Cosmochim. Acta 67, 2843–2856. doi:10.1016/S0016-7037(03)00089-9

732 Fallon, E.K., Petersen, S., Brooker, R.A., Scott, T.B., 2017. Oxidative dissolution of hydrothermal mixed-sulphide ore: An assessment of current knowledge in relation to seafloor massive sulphide mining. Ore Geol. Rev. 86, 309–337. doi:10.1016/j.oregeorev.2017.02.028

733 Feely, R.A., Lewison, M., Massoth, G.J., Robert-Baldo, G., Lavelle, J.W., Byrne, R.H., Von Damm, K.L., Curl, H.C., 1987. Composition and dissolution of black smoker particulates from active vents on the Juan de Fuca Ridge. J. Geophys. Res. 92, 11347–11363. doi:10.1029/JB092iB11p11347

736 Franklin, N.M., Stauber, J.L., Lim, R.P., 2001. Development of flow cytometry-based algal bioassays for assessing toxicity of copper in natural waters. Environ. Toxicol. Chem. 20, 160–170. doi:10.1002/etc.5620200118

737 Fullston, D., Fornasiero, D., Ralston, J., 1999. Zeta potential study of the oxidation of copper sulfide minerals. Colloids Surfaces A Physicochem. Eng. Asp. 146, 113–121. doi:10.1016/S0927-7757(98)00725-0

738 German, C.R., Petersen, S., Hannington, M.D., 2016. Hydrothermal exploration of mid-ocean ridges: Where might the largest sulfide deposits be forming? Chem. Geol. 420, 114–126. doi:10.1016/j.chemgeo.2015.11.006

740 Gilbert, T., King, B., Benfer, N., Terrens, G., 2008. Appendix 12: Modelling the dispersion of the returned water discharge plume from the Solwara 1 seabed mining project, Manus Basin, Papua New Guinea.

744 Gwyther, D., 2008. Environmental Impact Statement, Solwara 1 Project, in: Main Report Coffey Natural Systems. Brisbane.

746 Hannington, M., Herzog, P., Scott, S., Thompson, G., Rona, P., 1991. Comparative mineralogy and geochemistry of gold-bearing sulfide deposits on the mid-ocean ridges. Mar. Geol. 101, 217–248. doi:10.1016/0025-3227(91)90073-D

748 Hannington, M., Jamieson, J., 2011. Estimating the metal content of SMS deposits, in: Oceans. IEEE.

749 Hannington, M.D., de Ronde, C.E.J., Petersen, S., 2005. Modern seafloor tectonics and submarine hydrothermal systems, Economic Geology: One Hundredth Anniversary Volume: 1905-2005. Society of Economic Geologists. doi:10.1029/GM091p0115

750 Hannington, M.D., Jamieson, J., Monecke, T., Petersen, S., 2010. Modern Sea-Floor Massive Sulfides and Base Metal Resources: Toward an Estimate of Global Sea-Floor Massive Sulfide Potential. Soc. Econ. Geol. Spec. Publ. 15 15, 317–338.

751 Heidel, C., Tichomirowa, M., Junghans, M., 2013. Oxygen and sulfur isotope investigations of the oxidation of sulfide mixtures containing pyrite, galena, and sphalerite. Chem. Geol. 342, 29–43. doi:10.1016/j.chemgeo.2013.01.016

752 Herzig, P.M., Hannington, M.D., 1995. Polymetallic massive sulfides at the modern seafloor a review. Ore Geol. Rev. 10, 95–115. doi:10.1016/0169-1368(95)00009-7

755 Humphris, S.E., Herzog, P.M., Miller, D.J., 1996. 158: College Station, TX (Ocean Drilling Program). Proc. ODP, Init. Repts.

757 Humphris, S.E., Herzog, P.M., Miller, D.J., Alt, J.C., Becker, K., Brown, D., Brüggemann, G., Chiba, H., Fouquet, Y., Gemmel, J.B., Guerin, G., Hannington, M.D., Holm, N.G., Honnorez, J.J., Iturrino, G.J., Knott, R., Ludwig, R., Nakamura, K., Petersen, S., Reysenbach, A.-L., Rona, P.A., Smith, S., Sturz, A.A., Tivey, M.K., Zhao, X., 1995. The internal structure of an active sea-floor massive sulphide deposit. Nature 377, 713–716. doi:10.1038/377713a0

760 Jyothi, N., Sudha, K.N., Natarajan, K.A., 1989. Electrochemical aspects of selective bioleaching of sphalerite and chalcopyrite from mixed sulphides. Int. J. Miner. Process. 27, 189–203. doi:10.1016/0301-7516(89)90064-1

762 Koleini, S.M.J., Jafarian, M., Abdollahy, M., Aghazadeh, V., 2010. Galvanic Leaching of Chalcopyrite in Atmospheric Pressure and Sulfate Media: Kinetic and Surface Studies. Ind. Eng. Chem. Res. 49, 5997–6002. doi:10.1021/ie100017u

764 Koski, R.A., Munk, L., Foster, A.L., Shanks, W.C., Stillings, L.L., 2008. Sulfide oxidation and distribution of metals near abandoned copper mines in coastal environments, Prince William Sound, Alaska, USA. Appl. Geochemistry 23, 227–254. doi:10.1016/j.apgeochem.2007.10.007

766 Kwong, Y.T.J., Swerhorne, G.W., Lawrence, J.R., 2003. Galvanic sulphide oxidation as a metal-leaching mechanism and its environmental implications. Geochemistry Explor. Environ. Anal. 3, 337–343. doi:10.1144/1467-7873/03/013

768 Li, Z., Heping, L., Liping, X., 2006. Galvanic interaction between galena and pyrite in an open system. Chinese J. Geochemistry 25, 230–237. doi:10.1007/BF02840416

770 Liu, Q., Li, H., Zhou, L., 2008. Galvanic interactions between metal sulfide minerals in a flowing system: Implications for mines environmental restoration. Appl. Geochemistry 23, 2316–2323. doi:10.1016/j.apgeochem.2008.02.024

772 Liu, X., Millero, F.J., 2002. The solubility of iron in seawater. Mar. Chem. 77, 43–54. doi:10.1016/S0304-4203(01)00074-3

774 Lizama, H.M., Suzuki, I., 1991. Interaction of chalcopyrite and sphalerite with pyrite during leaching by Thiobacillus ferrooxidans and Thiobacillus thiooxidans. Can. J. Microbiol. 37, 304–311. doi:10.1139/m91-047

776 Majima, H., 1969. How oxidation affects selective flotation of complex sulphide ores. Can. Metall. Q. 8, 269–273.

777 Majuste, D., Ciminelli, V.S.T., Osseo-Asare, K., Dantas, M.S.S., 2012. Quantitative assessment of the effect of pyrite inclusions on chalcopyrite electrochemistry under oxidizing conditions. Hydrometallurgy 113–114, 167–176. doi:10.1016/j.hydromet.2011.12.020

779 Malmström, M., Collin, C., 2004. Sphalerite weathering kinetics: effect of pH and particle size. Proc. 11th Symp. Water-Rock Interact. 1, 849–852.

780 McBeth, J.M., Little, B.J., Ray, R.I., Farrar, K.M., Emerson, D., 2011. Neutrophilic iron-oxidizing "Zetaproteobacteria" and mild steel corrosion in nearshore marine environments. Appl. Environ. Microbiol. 77, 1405–1412. doi:10.1128/AEM.02095-10

782 McKibben, M.A., Barnes, H.L., 1986. Oxidation of pyrite in low temperature acid solutions: Rate laws and surface textures. Geochim. Cosmochim. Acta 50, 1509–1520. doi:10.1016/0016-7037(86)90325-X

784 Mehta, A.P., Murr, L.E., 1983. Fundamental studies of the contribution of galvanic interaction to acid-bacterial leaching of mixed metal sulfides. Hydrometallurgy 9, 235–256. doi:10.1016/0304-386X(83)90025-7

786 Mehta, A.P., Murr, L.E., 1982. Kinetic study of sulfide leaching by galvanic interaction between chalcopyrite, pyrite, and sphalerite in the presence of T. ferrooxidans (30°C) and a thermophilic microorganism (55°C). Biotechnol. Bioeng. 24, 919–40. doi:10.1002/bit.260240413

788 Millero, F.J., 2013. Chemical Oceanography, Fourth Edition. CRC Press.

789 Mills, R.A., Elderfield, H., 1995. Rare earth element geochemistry of hydrothermal deposits from the active TAG Mound, 26°N Mid-Atlantic Ridge. Geochim. Cosmochim. Acta 59, 3511–3524.

791 Monecke, T., Petersen, S., Hannington, M.D., Grant, H., Samson, I., 2016. The minor element endowment of modern sea-floor massive sulfide deposits and comparison with deposits hosted in ancient volcanic successions. Rev. Econ. Geol. 18, 245–306.

792 Moses, C.O., Herman, J.S., 1991. Pyrite oxidation at circumneutral pH. Geochim. Cosmochim. Acta 55, 471–482. doi:10.1016/0016-7037(91)90005-P

794

795 Moses, C.O., Kirk Nordstrom, D., Herman, J.S., Mills, A.L., 1987. Aqueous pyrite oxidation by dissolved oxygen and by ferric iron. *Geochim. Cosmochim. Acta* 51,
796 1561–1571. doi:10.1016/0016-7037(87)90337-1
797 Murr, L.E., 2006. Biological issues in materials science and engineering: Interdisciplinarity and the bio-materials paradigm. *JOM* 58, 23–33. doi:10.1007/s11837-
798 006-0136-3
799 Natarajan, K., 1988. Electrochemical aspects of bioleaching polysulfide minerals. *Miner. Metall. Process.* 5, 61–65.
800 Natarajan, K.A., 1985. Microbe-mineral interactions of relevance in the hydrometallurgy of complex sulphides, in: Mehrotra, S.P., Ramachandran, T.R. (Eds.),
801 *Progress in Metallurgical Research-Fundamental and Applied Aspects*. Tata McGraw Hill, New Delhi, New Delhi, pp. 105–112.
802 Natarajan, K.A., Iwasaki, I., 1983. Role of Galvanic Interactions in the Bioleaching of Duluth Gabbro Copper-Nickel Sulfides. *Sep. Sci. Technol.* 18, 1095–1111.
803 doi:10.1080/01496398308059919
804 Natarajan, K., Iwasaki, I., 1986. Microbe-mineral interactions in the leaching of complex Sulfides, in: Clum, J.A., Haas, L.A. (Eds.), *Microbiological Effects on*
805 *Metallurgical Processes*. TMS AIME, New York, New York.
806 Parry, D.L., 2008. Solwara 1 Project Elutriate Report Phase 1 and 2.
807 Plumlee, G., Logsdon, M., Filipek, L., 1999. The environmental geology of mineral deposits, in: *The Environmental Geochemistry of Mineral Deposits*. Society of
808 Economic Geologists, pp. 71–116.
809 Rimstidt, J.D., Chermak, J.A., Gagen, P.M., 1994. Rates of reaction of galena, sphalerite, chalcopyrite, and arsenopyrite with Fe (III) in acidic solutions, in: Alpers,
810 C.N., Blowes, D.W. (Eds.), *Environmental Geochemistry of Sulfide Oxidation*. American Chemical Society, Washington, DC, pp. 2–13. doi:10.1021/bk-1994-
811 0550.ch001
812 Rimstidt, J.D., Newcomb, W.D., 1993. Measurement and analysis of rate data: The rate of reaction of ferric iron with pyrite. *Geochim. Cosmochim. Acta* 57, 1919–
813 1934. doi:10.1016/0016-7037(93)90084-A
814 Romano, G.Y., 2012. Kinetics of Pyrrhotite Oxidation in Seawater: Implications for Mining Seafloor Hotspots.
815 Salmon, S.U., Malmström, M.E., 2006a. Quantification of mineral dissolution rates and applicability of rate laws: Laboratory studies of mill tailings. *Appl.*
816 *Geochemistry* 21, 269–288. doi:10.1016/j.apgeochem.2005.09.014
817 Salmon, S.U., Malmström, M.E., 2006b. Quantification of mineral dissolution rates and applicability of rate laws: Laboratory studies of mill tailings. *Appl.*
818 *Geochemistry* 21, 269–288. doi:10.1016/j.apgeochem.2005.09.014
819 Schlitzer, R., 2000. Electronic Atlas of WOCE Hydrographic and Tracer Data Now Available. *Eos Trans. AGU* 81.
820 Simpson, S., Angel, B., Hamilton, I., Spadaro, D., Binet, M., 2007. Water and Sediment Characterisation and Toxicity Assessment for the Solwara 1 Project.
821 Subrahmanyam, T.V., Forssberg, K.S.E., 1993. Mineral solution-interface chemistry in minerals engineering. *Miner. Eng.* 6, 439–454. doi:10.1016/0892-
822 6875(93)90173-K
823 Webber, A.P., Roberts, S., Murton, B.J., Hodgkinson, M.R.S., 2015. Geology, sulfide geochemistry and supercritical venting at the Beebe Hydrothermal Vent Field,
824 Cayman Trough. *Geochemistry, Geophys. Geosystems* 16, 2661–2678. doi:10.1002/2015GC005879
825 Weisener, C.G., Smart, R.S.C., Gerson, A.R., 2004. A comparison of the kinetics and mechanism of acid leaching of sphalerite containing low and high
826 concentrations of iron. *Int. J. Miner. Process.* 74, 239–249. doi:10.1016/j.minpro.2003.12.001
827 Wohlgemuth-Ueberwasser, C.C., Viljoen, F., Petersen, S., Vorster, C., 2015. Distribution and solubility limits of trace elements in hydrothermal black smoker
828 sulfides: An in-situ LA-ICP-MS study. *Geochim. Cosmochim. Acta* 159, 16–41. doi:10.1016/j.gca.2015.03.020
829 Yelloji Rao, M.K., Natarajan, K.A., 1989. Electrochemical effects of mineral-mineral interactions on the flotation of chalcopyrite and sphalerite. *Int. J. Miner. Process.*
830 27, 279–293. doi:10.1016/0301-7516(89)90069-0
831

832 10 Figure Captions

833 **Figure 1** A galvanic cell occurs when two sulphide minerals with different rest potentials are coupled together in a
834 solution that acts as an electrolyte (seawater in this case). The mineral with the higher rest potential behaves as a
835 cathode (e.g. pyrite) and is galvanically protected with the reduction reaction occurring on its surface. The mineral
836 with the lower rest potential (e.g. chalcopyrite) behaves as an anode and is preferentially dissolved with oxidative
837 dissolution occurring on its surface. There are a number of potential reduction reactions that occur on the surface
838 of the cathode depending on the ions available; shown above are the formation of water as well as hydroxides that
839 can then ultimately form Fe hydroxides/oxy-hydroxides if ferrous Fe is available. Figure adapted from Murr (2006)
840 and Fallon et al. (2017). Rest potentials of minerals at pH 4 are taken from Majima (1969) and references therein;
841 quoted where available are rest potentials of minerals at pH 7 in distilled water, taken from Cheng and Iwasaki
842 (1992).

843 **Figure 2** The location of TAG samples used in this study. TAG-B is located in the TAG-3 area and TAG H and J in
844 the TAG-4 area. Detailed bathymetric data is overlaid on the map and the inset shows the location of the TAG
845 hydrothermal field within the context of the Atlantic Ocean. This figure is reproduced from Humphris et al. (1995).

846 **Figure 3** Back-scattered electron (BSE) and reflected light microscopy photographs (PP, plane polarised; XP,
847 cross polarised) of samples. TAG-B is a heavily oxidised, brecciated sample containing a high abundance of
848 quartz, largely coated in silica and oxidation products including Fe oxides and Fe oxy-hydroxides (limonite).
849 Included in this are grains of pyrite and chalcopyrite, with rare sphalerite. TAG-H is dominantly pyrite and
850 marcasite with sphalerite veinlets and inclusions. TAG-J is similar with major pyrite and marcasite (less marcasite
851 than TAG-H), however contains major chalcopyrite and no sphalerite. *py*, pyrite; *ccp*, chalcopyrite; *mc*, marcasite;
852 *sph*, sphalerite; *qtz*, quartz

853 **Figure 4** Reflected light microscope (plane polarised) images of cleaned powders (2.5 - 45 μm). Presence of
854 inclusions shows their preservation from whole rock sample through the grinding and sieving process. Chalcopyrite
855 inclusions are observed in pyrite grains of both TAG B (top) and TAG J (bottom). Contacts between pyrite-
856 chalcopyrite and sphalerite-chalcopyrite in TAG B and covellite-chalcopyrite in TAG-J are also observed. TAG-H
857 has common sphalerite-pyrite contacts. Whilst inclusions have been identified in grains of the ore powders, no
858 quantifiable number can be assigned.

859 **Figure 5a, b and c** Cu, Fe and Pb leached over time with all samples. Concentrations have been corrected to
860 remove initial starting concentrations of Fe, Cu and Pb in seawater and normalised to mass of ore, volume of
861 seawater used and surface area of each respective sample and are presented in $\mu\text{mol}/\text{m}^2$. Shown for reference
862 are representative maximum solubility's of Cu, Fe and Pb in seawater taken from experimental and calculation
863 studies (Angel et al., 2015; Franklin et al., 2001; Liu and Millero, 2002). Only Fe exceeds its solubility limit, which is
864 expected based on the pH of the system and is supported by observations of Fe oxide/oxy-hydroxide precipitation.

865 **Figure 6a, b and c** Cu, Fe and Pb leached over time with all samples. Concentrations have been corrected to
866 remove initial starting concentrations of Fe, Cu and Pb in seawater and have been normalised to mass of each
867 respective sample and are presented in ppb. Shown for comparison is elutriate data produced by Nautilus Minerals
868 for the EIS (Parry, 2008; Simpson et al., 2007). Pink stars are data from an experiment undertaken with
869 'representative' Fe-rich Solwara 1 ore at 6 °C, particle size of 3.35 mm and a fluid to rock ratio of 25g to 250 mL
870 (100 g/L) of seawater (Parry, 2008). Cyan crosses are data from an experiment with a Cu-Zn-Pb rich ore at 22 °C,
871 particle size of <0.25 mm and a fluid to rock ratio of 1.25 g to 125 mL (10 g/L) of seawater (Simpson et al., 2007).
872 Solid lines represent absolute concentrations and dashed lines represent concentration (ppb) data scaled to 2 g/L
873 (ore to seawater ratio) for comparison with experiments undertaken in this study. No corrections can be made to
874 scale EIS concentrations for temperature and grain size in order for comparison with this study.

875 **Figure 7** The dissolved Cu, Fe and Pb shown in experiments from this study as a percentage of the bulk
876 concentration. Shown for comparison is the dissolved Cu, Fe and Pb as a percentage of the bulk from elutriate
877 data produced by Nautilus Minerals for the EIS. Hatched bars indicate concentrations that have been corrected to
878 2 g/L rock to fluid ratio, in line with this study. a) Initial loss of bulk as a %, at the 10-minute sampling interval. b)
879 Dissolved concentrations as a % of the bulk, taken as an average after the 30-minute sampling interval.

880
881

882 **Table 1** Sample list with quoted surface area from BET measurements of ground, sieved and cleaned sulphide ore powders (<45µm). Semi
883 quantitative data (Wt %) are presented based on powder x-ray diffraction of ground, sieved and cleaned sulphide ore powders (<45µm),
884 dashes indicate either no observation or that the concentration was below the detection limit. Also presented are observations of inclusions
885 based upon reflected light microscopy and SEM, EDX. Abbreviations used here are *Py* (pyrite), *Mc* (marcasite), *Ccp* (chalcopyrite), *Cv*
886 (covellite), *Sp* (sphalerite), *Anh* (anhydrite), *Ox* (Fe oxides/oxy-hydroxides) and *qtz* (quartz). Bulk Fe, Cu and Pb concentration determined
887 by aqua regia digestion with ICP-OES. Detailed method of acid digestion included in Supplementary Material D.

Location	Sample	Surface Area (m ² /g)	Mineral Abundances (wt %)								Inclusions	Bulk Fe	SD	Bulk Cu	SD	Bulk Pb	SD
			Py	Mc	Ccp	Cv	Sp	Anh	Ox	Qtz		wt%	ppm	ppm	ppm		
TAG-3	TAG-B	1.843	24.4	--	6.2	--	--	--	5.5	63.9	ccp in py, py in ccp	25.8	1.0	43035	5	182.73	6.84
TAG-4	TAG-H	0.552	37.4	42.0	0.9	--	1.2	0.8	--	17.7	sp in py, mc	44.4	3.8	1130	86	107.97	9.12
TAG-4	TAG-J	0.607	83.8	5.9	5.6	1.4	0.6	--	--	2.6	sp, ccp in py	45.3	5.3	36592	4073	164.05	19.20

888

889

890

891

892

893

894

895

896

897

898

899

900

901

902 **Table 2** Average concentration of Fe, Cu and Pb within pyrite, marcasite and sphalerite. Concentrations determined by laser ablation inductively
 903 coupled mass spectrometry (LA-ICP-MS). N refers to number of analyses. For detailed LA-ICP-MS methodology, please refer to Supplementary
 904 Material B.

Sample	Phase	N	Fe wt%	Error	Cu ppm	Error	Pb	Error
TAG-B	Pyrite	4	56.90	2.41	461.20	49.83	11.30	0.68
TAG-H	Pyrite	8	54.21	2.07	33.15	3.67	73.34	4.35
TAG-H	Marcasite	8	55.62	1.87	70.75	4.79	113.59	10.58
TAG-H	Sphalerite	3	0.79	0.02	1720.70	28.35	212.00	6.01
TAG-J	Pyrite	6	57.34	2.64	715.30	43.48	217.30	15.90
TAG-J	Marcasite	3	57.31	1.59	77.20	5.75	65.70	5.29

905
 906
 907
 908 **Table 3** Run parameters for experiments conducted in this study. Temperature, oxygen concentration and conductivity are averages of all
 909 measurements taken over the course of the run. Dissolved oxygen concentrations were held constant across the duration of experiments. The
 910 error reported is the standard deviation between those values.

Run	T	Sample	Size	Initial Mass	Mass lost on probes	Mass during run	Average Dissolved Oxygen Concentration	Initial pH	Final pH	Conductivity
	°C		µm	g	g	g	mg L ⁻¹			mS cm ⁻¹
16	11.8 +/- 0.6	TAG-B	2.5 - 45	1.0023	0.0382	0.9641	9.4 +/- 0.04	8.05	7.13	37.9 +/- 0.2
18	13.0 +/- 1.4	TAG-H	2.5 - 45	0.5939	0.0378	0.5561	9.8 +/- 0.70	8.91	7.79	36.5 +/- 0.2
19	11.5 +/- 1.0	TAG-J	2.5 - 45	0.9106	0.0682	0.8424	8.96 +/- 0.90	8.4	7.56	38.6 +/- 0.6

911
 912
 913
 914

